

# A binary electrolyte model of a cylindrical alkaline cell

J.J. Kriegsmann, H.Y. Cheh \*

*Department of Chemical Engineering and Applied Chemistry, Columbia University, 500 West 120th Street, New York, NY 10027, USA*

Received 27 May 1999; accepted 6 June 1999

## Abstract

A cylindrical alkaline cell is modeled as a binary electrolyte system by assuming the direct electrochemical formation of ZnO in the anode. Justifications for replacing the dissolution–precipitation mechanism are provided. Compared to the original model, the binary electrolyte model has a more understandable model formulation, more consistent physical property data, and greater flexibility in certain instances. The binary electrolyte model predicts a longer cell life and higher operating voltage than the ternary electrolyte model for the test case discharge rate. There are no numerical difficulties associated with the zincate ion in the binary electrolyte model, because this species is not considered. The characteristics and advantages of the simplified anode behavior are discussed. An application of the binary electrolyte model is included. © 2000 Elsevier Science S.A. All rights reserved.

*Keywords:* Alkaline batteries; Zincate ion; Zinc oxide; Precipitation rate; Discharge time

## 1. Introduction

The mathematical model presented by Podlaha and Cheh [1,2] for a Zn/MnO<sub>2</sub> cylindrical alkaline cell has been revised in two previous studies [3,4]. In the first study [3], the initial cathode specific interfacial area was raised to match the literature values for this quantity. More appropriate data were used in the second study [4] to develop a new correlation for the equilibrium zincate ion concentration. Both investigations resulted in longer simulated discharge times with respect to a base case design, using a test discharge scheme. The revised cathode specific interfacial area gives a much longer discharge time than the base case design. The new equilibrium zincate ion correlation leads to a slightly longer discharge time compared to the base case design, although the effect of this revision is much less than the change in the cathode surface area.

Both analyses encountered numerical difficulties involving the zincate ion concentration as it approaches zero in a localized region of the cell. Because the model uses concentrated ternary electrolyte theory, the mathematical formulation leads to a logarithmic singularity when the zincate ion is completely depleted anywhere in the cell. Nonphysical voltage fluctuations result from this calcula-

tion. The model should have a smooth cell voltage transition as the zincate ion concentration approaches zero. However, such a scheme is not available. A numerical remedy has been developed [4], but it is not acceptable on a physical basis because the ternary form of Ohm's law in the electrolyte phase is replaced with a pseudo-binary form.

It is instructive to consider modeling this system as a binary electrolyte before employing other numerical procedures to eliminate these problems. Chen and Cheh [5,6] used concentrated binary electrolyte theory under two scenarios for the Zn/MnO<sub>2</sub> system. In the mixed-reaction anode model [5], the anode is considered a "black box", and Zn is allowed to form solid ZnO and zincate ion in parallel, but in different proportions set by an arbitrary parameter. The electrolyte is modeled as a binary system. A complete cell development is used with the dissolution–precipitation anode model [6], where Zn forms zincate ion through an oxidation reaction, prior to the chemical precipitation of ZnO. Only the anode is modeled as a ternary electrolyte, since binary electrolyte theory is used in the separator and cathode. The Zn/MnO<sub>2</sub> system has not been described as a complete cell assembly using binary electrolyte theory, considering only direct ZnO formation in the anode. The zincate ion has always been included when formulating the tertiary current distribution case.

A binary electrolyte model for this system may provide valuable information. The motivation is the success of

\* Corresponding author. Tel.: +1-212-854-4453; fax: +1-212-854-3054; E-mail: hyc1@columbia.edu

simplified models [7–13] used with established mathematical models of porous electrodes in lithium battery systems [14–16]. The goal of this study is to model the Zn/MnO<sub>2</sub> system as a concentrated binary electrolyte. This model may serve as a useful benchmark in addressing the effect of the zincate ion. For primary, high-rate discharges the binary model may replace the ternary model because the adverse shape change effects upon secondary operation [17–22], where the zincate ion is important, should not limit the cell performance. Justifications for the rational application of a binary electrolyte model for this system are provided. An application of the binary model is shown in order to demonstrate its utility in screening certain model parameters, for a case where the ternary model has numerical problems.

## 2. Justifications

A main problem of the ternary electrolyte model is the complexity of the anode formulation, which is adapted from Sunu [23], and Sunu and Bennion [19]. The equations describing the mixed-control assumption of the zincate ion mass transfer rate and the ZnO chemical precipitation rate are difficult to understand. Also, the initial values of the aqueous salt mass transfer coefficients and the chemical rate constant for precipitation of ZnO constitute a large number of arbitrary parameters. Chen and Cheh [5] used less arbitrary parameters with the mixed-reaction anode model. The main parameter describes the extent of direct Zn conversion to ZnO, relative to the total Zn conversion. For simulations of D-size cells, the cell voltage profiles match the experimental data best when direct ZnO formation is about 80% of the total Zn conversion.

Ternary data for the KOH/K<sub>2</sub>Zn(OH)<sub>4</sub> (potassium zincate)/H<sub>2</sub>O system at high concentrations are lacking. The ternary activity coefficients are estimated using Newman's development [23,24], where data for K<sub>2</sub>Zn(OH)<sub>4</sub> are replaced with values for potassium chromate [23]. The expressions are complicated and the coefficients vary by several orders of magnitude with hydroxyl ion concentrations encountered in normal simulations. However, much experimental data are available for the binary KOH system [1].

The mixed-control formulation in the precipitation analysis for the anode is not applied in the separator. This is an oversimplification because the inert, porous solid in the separator should provide nucleation sites, as do the solid particles in the anode [25]. The rate constant for the separator precipitation reaction is equivalent to the chemical rate constant for precipitation, because an effective rate constant is not calculated. The rate constant for precipitation in the separator is an order of magnitude larger than the effective rate constant in the anode [4]. There is a bias in the model for predicting a very large amount of precipitation in the separator, especially near the anode/separator

interface. Thus, the transport limitations ascribed to the low porosity in the separator, due to precipitation of ZnO, may be overstated.

The zincate ion concentration is coupled to the cell polarization mainly through the ternary form of Ohm's law in the electrolyte phase, in what are referred to as the concentration overpotential terms, and also in the anode electrochemical kinetics. There is small dependence on the ionic concentrations and the local overpotential in the Butler–Volmer expression for the transfer current in the anode. This was observed in an earlier study [4]. The reason for this small dependence is a large exchange current density for the oxidation reaction of Zn to form zincate ion. The transfer current in the anode is large and nonuniform, but the polarization is small. The ternary form of Ohm's law in the electrolyte phase is thus the main embodiment of ternary electrolyte theory in the model. When a pseudo-binary form of Ohm's law in the electrolyte phase is used to eliminate the numerical problems [4], neglecting the zincate ion concentration overpotential has almost no effect on the operating voltage. A very low transference number for the zincate ion indicates that the current density contribution from this species is minor. It is expected that the coupling between the cell polarization and the zincate ion concentration is negligible, except in the case of the numerical singularity.

It is now shown that the zincate ion can be neglected because the precipitation of ZnO is very fast in comparison to the diffusion of the zincate ion in the cell. For the precipitation reaction, the appropriate time scale is the half-life period [26]. Since first-order precipitation kinetics are used in the model, the anode precipitation time scale,  $t_{p,a}$ , is approximated by

$$t_{p,a} = \frac{1}{a_a^0 k_s^0} \ln 2 \quad (1)$$

and the separator precipitation time scale,  $t_{p,s}$ , is estimated from

$$t_{p,s} = \frac{1}{a_s^0 k_x} \ln 2 \quad (2)$$

where  $a_a^0$  is the initial specific surface area for the precipitation reaction in the anode,  $k_s^0$  is the initial effective rate constant for the ZnO precipitation reaction in the anode,  $a_s^0$  is the initial specific surface area for the precipitation reaction in the separator, and  $k_x$  is the chemical rate constant for the ZnO precipitation reaction.

These quantities are compared with the time constants for the diffusion of zincate ion in the anode and separator. The time scale for diffusion of zincate ion in the anode,  $t_{diff,a}$ , is given by [27]

$$t_{diff,a} = \frac{(r_a - r_{ac})^2}{(\epsilon_a^0)^{0.5} D_A} \quad (3)$$

Table 1  
Quantities used in justifying the binary electrolyte model

$R_{p,a}^0$	$0.2 \times 10^{-5} \text{ mol/cm}^3 \text{ s}$ [4]
$R_{p,s}^0$	$0.1 \times 10^{-4} \text{ mol/cm}^3 \text{ s}$ [4]
$c_1^0$	$6.95 \times 10^{-4} \text{ mol/cm}^3$ [4]
$D_A$	$6.9 \times 10^{-6} \text{ cm}^2/\text{s}$ [1]
$r_{ac}$	0.09 cm [1]
$r_a$	0.43 cm [1]
$r_s$	0.45 cm [1]
$\epsilon_a^0$	0.74 [1]
$\epsilon_s^0$	0.8 [1]
$a_a^0$	$50.0 \text{ cm}^{-1}$ [1]
$a_s^0$	$30.0 \text{ cm}^{-1}$ [1]
$k_s^0$	$2.17 \times 10^{-4} \text{ cm/s}$ [4]
$k_x$	0.005 cm/s [1]

and the time scale for diffusion in the separator,  $t_{\text{diff},s}$ , is computed from

$$t_{\text{diff},s} = \frac{(r_s - r_a)^2}{(\epsilon_s^0)^{0.5} D_A} \quad (4)$$

where  $r_a$  is the anode/separator interface location,  $r_{ac}$  is the anode current collector location,  $\epsilon_a^0$  is the initial anode porosity,  $D_A$  is the diffusion coefficient of potassium zincate,  $r_s$  is the separator/cathode interface location, and  $\epsilon_s^0$  is the initial separator porosity. Table 1 lists the values needed to calculate the four time constants, for a base case AA-size design [1–4].

For the anode,  $t_{p,a} = 64.0 \text{ s}$  and  $t_{\text{diff},a} = 19.7 \times 10^3 \text{ s}$ , and the precipitation reaction is much faster than the diffusion of zincate ion in this region. Similarly,  $t_{p,s} = 4.62 \text{ s}$  and  $t_{\text{diff},s} = 64.8 \text{ s}$ , so that the diffusion time scale is at least an order of magnitude larger than the precipitation time scale in the separator. These values support the assumption of fast ZnO precipitation that can be approximated by the direct electrochemical conversion of Zn to ZnO. The cell discharge time is implicit in this analysis. With a discharge time on the order of  $10^3 \text{ s}$  for a high-rate discharge of an AA-size cell with a 0.8-V cutoff voltage,

diffusion on the length scale of an electrode is slow and precipitation is rapid.

Damköhler numbers are generated based on the precipitation reaction rates in the anode and separator. For the anode, the Damköhler number,  $Da$ , is estimated with [27,28]

$$Da = \frac{R_{p,a}^0 (r_a - r_{ac})^2}{(\epsilon_a^0)^{0.5} D_A c_1^0} \quad (5)$$

and for the separator  $Da$  is calculated from

$$Da = \frac{R_{p,s}^0 (r_s - r_a)^2}{(\epsilon_s^0)^{0.5} D_A c_1^0} \quad (6)$$

where  $R_{p,a}^0$  is a characteristic value of the precipitation rate in the anode,  $c_1^0$  is the initial zincate ion concentration, and  $R_{p,s}^0$  is a characteristic value of the precipitation rate in the separator. Table 1 also lists the additional quantities for use in these two calculations.

The results are  $Da = 56.7$  for the anode and  $Da = 0.933$  for the separator. The precipitation rate is much larger than the diffusion rate in the anode, and they are the same order of magnitude in the separator.  $Da$  for the anode is more important because this is the region where zincate ion is produced by the electrochemical reaction. The value for the anode also supports the validity of assuming the direct electrochemical production of ZnO, rather than the dissolution–precipitation mechanism. The binary electrolyte model is now presented.

### 3. Binary electrolyte model

The notation used with the binary electrolyte model conforms to earlier studies dealing with the application [29,30] and revision [3,4] of the original model [1]. The schematic for a cylindrical alkaline cell is given in Fig. 1. The radial locations denote the important interfacial

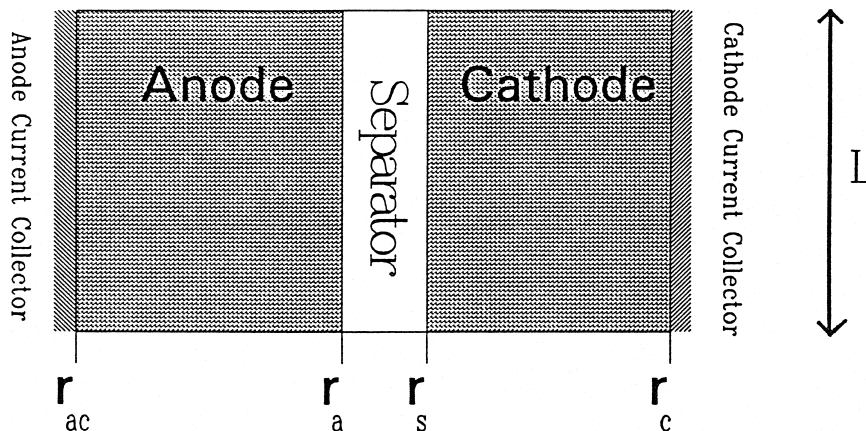


Fig. 1. Schematic for a cylindrical Zn/MnO<sub>2</sub> alkaline cell.

boundaries of the cell. The cell height is  $L$ . Further details of the system are available in Ref. [1].

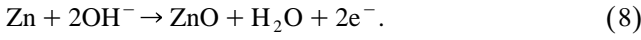
### 3.1. Material balance in the electrolyte phase

For the binary KOH electrolyte, the general molar flux of hydroxyl ion,  $N_2$ , is given by [31,32]

$$N_2 = -D_B \epsilon^{1.5} \nabla c_2 + \frac{t_2}{z_2 F} \mathbf{i}_2 + c_2 \mathbf{v} \quad (7)$$

where  $c_2$  is the hydroxyl ion concentration,  $D_B$  is the diffusion coefficient of aqueous KOH,  $\epsilon$  is the porosity,  $t_2$  is the transference number of hydroxyl ion with respect to the volume average velocity,  $z_2$  is the charge number of the hydroxyl ion,  $\mathbf{i}_2$  is the superficial current density in the electrolyte phase, and  $\mathbf{v}$  is the volume average velocity of the electrolyte. The binary value of  $t_2$  is given in Ref. [1]. The expression for  $D_B$  in the ternary model is based on binary electrolyte data, so no alteration is needed. The notation for  $\epsilon$  changes depending on the cell region as follows: in the anode  $\epsilon = \epsilon_a$ , in the separator  $\epsilon = \epsilon_s$ , and in the cathode  $\epsilon = \epsilon_c$ .

The major adjustment to the original model is the assumption of the direct oxidation of Zn to form ZnO in the anode. There is no precipitation in the revised model. The new anode reaction is



The hydroxyl ion stoichiometry is changed in the anode and separator. The material balance in the anode is now

$$\frac{\partial \epsilon_a c_2}{\partial t} = -\nabla \cdot N_2 - \frac{j_a}{F} \quad (9)$$

where  $j_a$  is the transfer current or electrochemical reaction rate in the anode. The material balance in the separator is revised through

$$\frac{\partial \epsilon_s c_2}{\partial t} = -\nabla \cdot N_2 \quad (10)$$

where there is no source term because the precipitation reaction is not considered. No revision of the original model is necessary for the hydroxyl ion material balance in the cathode.

### 3.2. Ohm's law in the electrolyte phase

The general form of Ohm's law in the electrolyte phase for the binary KOH system is described by [31–33]

$$\nabla \eta = \mathbf{i}_2 \left( \frac{1}{\kappa \epsilon^{1.5}} + \frac{1}{\sigma} \right) - \frac{\mathbf{I}}{\sigma} + \frac{\nu_e RT}{nF} \left( \frac{s_2}{\nu_{2B}} + \frac{nt_2}{z_2 \nu_{2B}} - \frac{s_0}{c_0} c_2 \right) \nabla \ln(f_B c_2) \quad (11)$$

where  $\eta$  is the local overpotential,  $\kappa$  is the electrolyte conductivity,  $\sigma$  is the effective matrix conductivity,  $\mathbf{I}$  is

the cell current density vector,  $\nu_e$  is the number of ions that form when KOH dissociates,  $T$  is the cell temperature,  $n$  is the number of electrons transferred in the arbitrary reference electrode reaction,  $\nu_{2B}$  is the number of hydroxyl ion molecules that can dissociate from KOH,  $c_0$  is the solvent concentration, and  $s_i$  is the stoichiometric coefficient of species  $i$  in the arbitrary reference electrode reaction. The mean molar activity coefficient of the KOH electrolyte is given by  $f_B$ . The form for  $f_B$  is listed in Ref. [1]. The ternary model uses the binary form of Sunu [23] for  $\kappa$ , and it is not changed for the binary model. In the separator,  $\mathbf{I}$  and  $\mathbf{i}_2$  are related in such a way that the terms involving  $\sigma$  cancel out. In the cathode, the same solid solution terms present in Ref. [1] are retained, but they are not shown here. In the anode, the reference electrode is the same as the Zn electrode. A MnO<sub>2</sub> reference electrode is used for the separator and cathode forms of Eq. (11).

### 3.3. Electrolyte convection

The expressions that are shown in Refs. [31,32] for the volume average velocity in the electrolyte phase are applied to this system. For the anode, convection is determined by

$$\frac{\partial \epsilon_a}{\partial t} + \nabla \cdot \mathbf{v} = (2\bar{V}_e(t_2 - 1) + \bar{V}_0) \frac{j_a}{2F} \quad (12)$$

where  $\bar{V}_e$  is the partial molar volume of aqueous KOH, and  $\bar{V}_0$  is the partial molar volume of the solvent in the KOH solution. Since there is no shape change in the separator region, the governing equation becomes

$$\nabla \cdot \mathbf{v} = 0 \quad (13)$$

For the cathode, the new form is

$$\frac{\partial \epsilon_c}{\partial t} + \nabla \cdot \mathbf{v} = (\bar{V}_e(t_2 - 1) + \bar{V}_0) \frac{j_c}{F} \quad (14)$$

where  $j_c$  is the transfer current in the cathode. The values for  $\bar{V}_e$  and  $\bar{V}_0$  are found in the original model, and the form for  $j_c$  is not changed.

### 3.4. Porosity variation

The anode porosity now varies according to

$$\frac{\partial \epsilon_a}{\partial t} = (\bar{V}_{\text{Zn}} - \bar{V}_{\text{ZnO}}) \frac{j_a}{2F} \quad (15)$$

where  $\bar{V}_{\text{Zn}}$  is the partial molar volume of Zn, and  $\bar{V}_{\text{ZnO}}$  is the partial molar volume of ZnO, which are both listed in the original model. The separator porosity is now constant because there is no precipitation reaction, so that

$$\epsilon_s = \epsilon_s^0 \quad (16)$$

where  $\epsilon_s^0$  is the initial separator porosity from the original model. There is no revision to the governing cathode porosity equation.

### 3.5. Electrochemical kinetics

A new expression for the anode electrochemical reaction rate is needed. The expression for the cathode transfer current is not changed. The form in the anode is chosen as [32]

$$j_a = a_a i_0 \left[ \left( \frac{c_2}{c_{2,\text{ref}}} \right)^2 \exp\left( \frac{\alpha_a F}{RT} \eta \right) - \exp\left( -\frac{\alpha_c F}{RT} \eta \right) \right] \quad (17)$$

where  $a_a$  is the specific interfacial area in the anode,  $i_0$  is the exchange current density evaluated at a reference condition for the anode reaction, and  $\alpha_a$  and  $\alpha_c$  are the transfer coefficients for the electrochemical reaction.

Two electrons are transferred in the anode reaction, and  $\alpha_a$  and  $\alpha_c$  are both chosen as 1.0. The use of two different anode specific areas is discarded. The simpler specific area function is retained because low polarization is expected in the anode and the higher-end expression will suffice. The  $a_a$  expression has the following form [1]

$$a_a = a_a^0 \left( \frac{1 - \epsilon_a}{1 - \epsilon_a^0} \right)^{2/3} \quad (18)$$

where  $a_a^0$  is the initial specific surface area in the anode, and  $\epsilon_a^0$  is the initial anode porosity. The base case  $a_a^0$  value is chosen as  $50 \text{ cm}^{-1}$ , and it is the same as the original model value. The value for  $i_0$  is also the same as

in Ref. [1]. Elementary kinetics are assumed, and the form for  $j_a$  is similar to the expression of Fan [32] for the Cd electrode discharge transfer current.

### 3.6. Initial and boundary conditions

With the exception of conditions involving the zincate ion concentration, which is removed from the model, all initial and boundary conditions are identical to those shown in Ref. [1].

## 4. Results

The binary electrolyte model is solved using a pentagonal BAND(J) subroutine [24,34] with a modified numerical linearization subroutine [33,35] and the Crank–Nicolson method. The results for an AA-size base case design that was used in earlier work with the Zn/MnO<sub>2</sub> system [1,3,4,29,30] are used to present the new model characteristics. The test discharge rate of 1.0 A and the 0.8-V cutoff voltage also conform to the previous studies. All of the parameters that are not altered here are the same values as in Ref. [1]. The revised value of the initial cathode specific interfacial area [3] is used, with  $a_c^0 = 6.03 \times 10^4 \text{ cm}^{-1}$ .

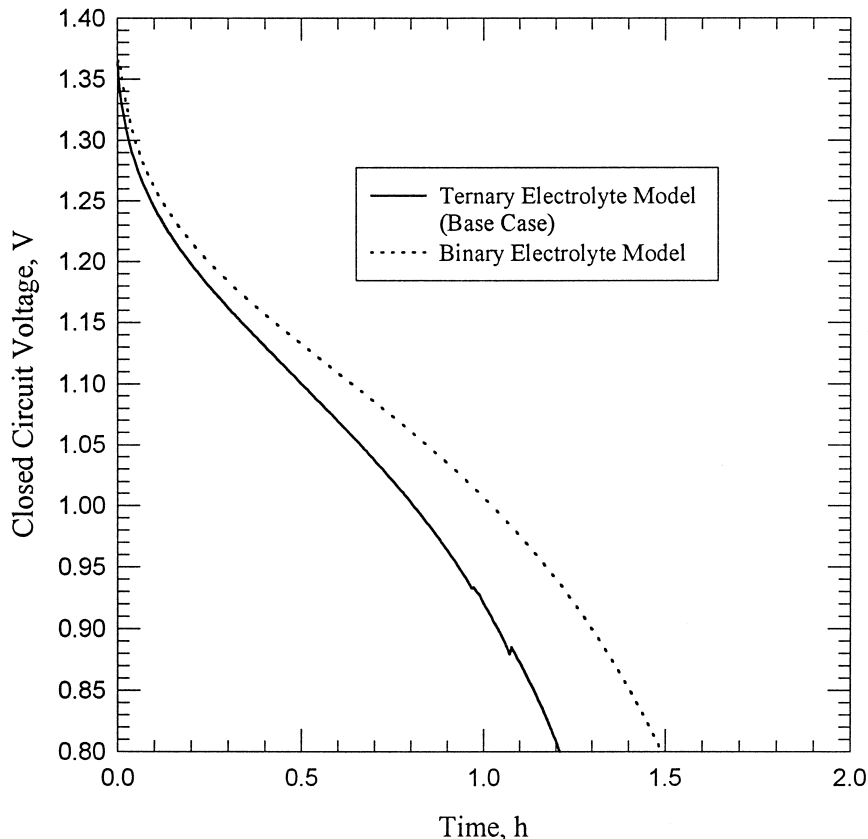


Fig. 2. Cell voltage curves for the binary electrolyte model and the original model.

Fig. 2 shows the cell voltage curve for the binary electrolyte model compared with the ternary model or base case curve. The base case ternary model is the most recent revision without any correction for the ternary to binary electrolyte transition voltage fluctuations [4], which are visible in Fig. 2. The discharge time,  $t_d$ , is longer for the binary model and the operating voltage is higher than the base case at all times. The discharge time for the base case is 1.211 h. The binary model has  $t_d = 1.489$  h, which is 23% longer than the base case. There are no voltage fluctuations with the binary model curve. The zincate ion is responsible for these discrepancies in the ternary model [3,4], but the absence of the zincate ion avoids these numerical problems.

The transfer current profiles throughout the cell are shown in Fig. 3. The reaction rate is large and nonuniform in the anode, especially near the anode/separator interface. At longer times, the transfer current in the anode reaches maximum values greater than  $3.5 \text{ A/cm}^3$ . This number is significantly larger than the maximum base case value. Near the anode/separator interface,  $j_a$  increases from the initial value. But the current distribution is more uniform and lower than the initial value at this interface for the base case at longer times [4]. This difference is attributed to the larger specific area values used in the expression for  $j_a$ , and also hydroxyl ion concentration

profiles that do not decrease in the anode. The transfer current throughout most of the anode is very small in comparison to the values near the anode/separator interface. The anode reaction is isolated to the interface with little movement to the anode interior. The transfer current profiles in the cathode are similar to the base case. The cathode profiles do not warrant further discussion because the cathode electrochemical kinetics have minimal coupling to the zincate ion in the ternary model.

Fig. 4 displays the local overpotential profiles throughout the cell. The binary model predicts very low polarization in the anode. The base case  $\eta$  values in the anode are close to 0.05 V at longer times, and this difference may explain the higher operating voltages compared to the base case. The low  $\eta$  values in the anode are due to the higher anode specific area values and the larger, and nearly constant, hydroxyl ion concentration profiles in the anode. The influence of the anode specific surface area and the hydroxyl ion concentration on  $\eta$  can also be seen in the expression for  $j_a$ . The anode profiles are uniform and close to zero, which approximate the original assumption of a “black box” anode with no polarization [5]. However, the binary model provides more detailed current distribution information. The profiles for the separator and cathode are similar to the base case, and no analysis is required because the zincate ion does not have much influence on

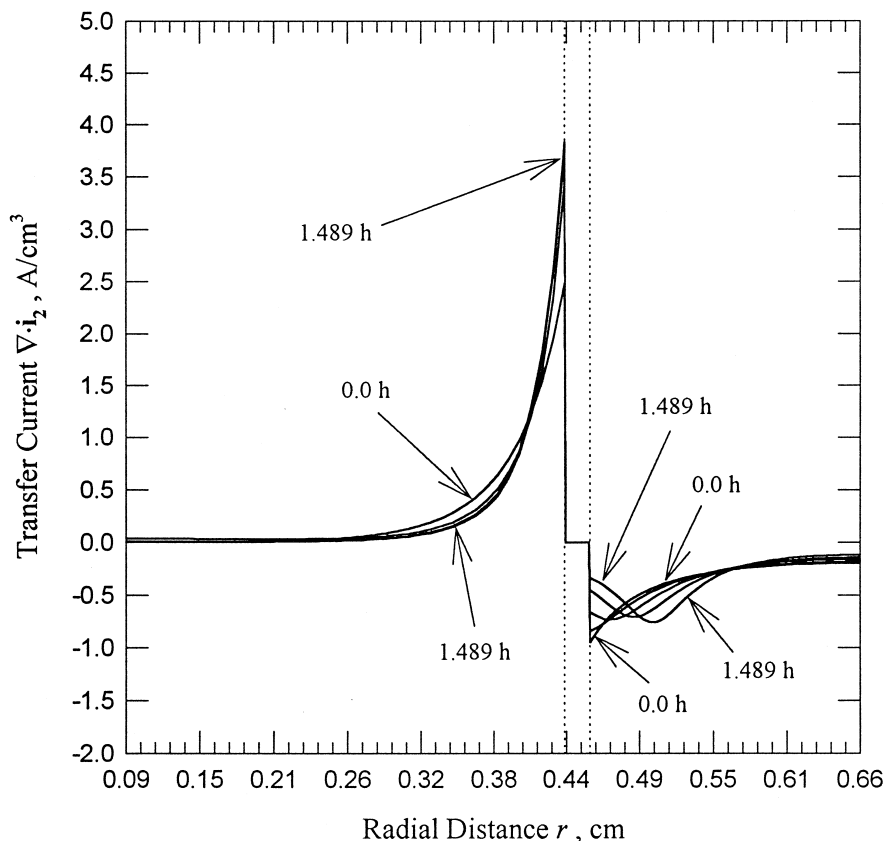


Fig. 3. Transfer current profiles calculated with the binary electrolyte model.

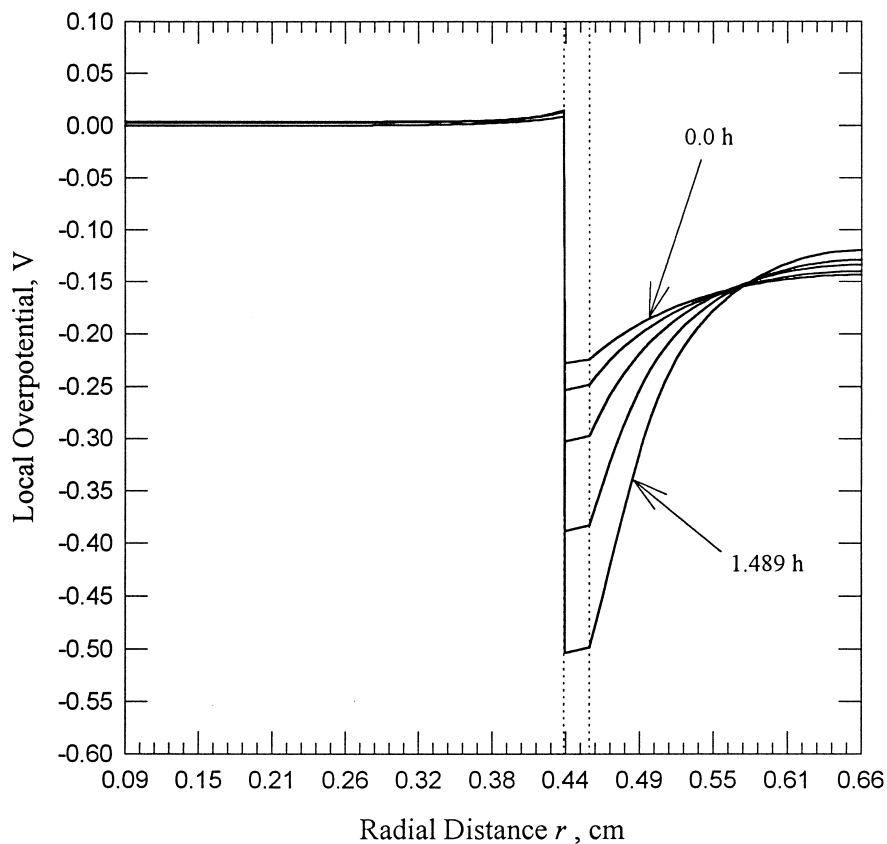


Fig. 4. Local overpotential profiles calculated with the binary electrolyte model.

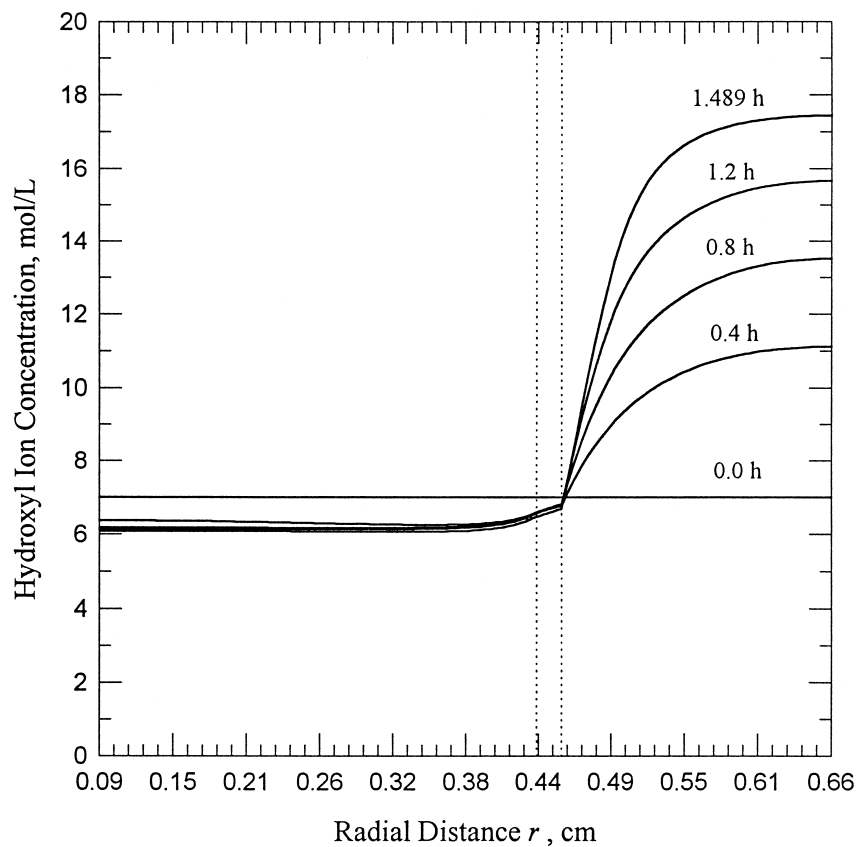


Fig. 5. Hydroxyl ion concentration profiles calculated with the binary electrolyte model.

Ohm's law in the electrolyte phase in the base case model. The influence of the hydroxyl ion concentration gradient on the separator and cathode polarization cannot be neglected in the same way.

Fig. 5 presents the hydroxyl ion concentration profiles throughout the cell. The large concentration gradients remain in the cathode, but the most important characteristics are the nearly uniform and constant profiles in the anode. The concentration in the anode is close to the initial value for the entire discharge. This is a large change from the base case, where there is continuous depletion of hydroxyl ion in the anode. The profiles are first explained by the new anode stoichiometry that leads to an overall cell balance with no hydroxyl ion depletion under equilibrium conditions. Larger concentrations result. Near the anode/separator interface, the flux of hydroxyl ion into the anode, because of the large concentration gradient in the cathode, is balanced by the large anodic transfer current that consumes hydroxyl ion. The small transfer current within the anode implies a low consumption rate of hydroxyl ion in the interior. Thus, the concentration in the anode is nearly constant.

Fig. 6 displays the volume average velocity profiles throughout the cell. At all times except for the start of discharge, the profiles are relatively invariant. The velocity profiles are similar in appearance to the ternary model

results, with the main differences occurring in the anode. The binary model predicts much lower velocities in the interior of the anode, away from the anode/separator interface. The explanation for this is the removal of the dissolution–precipitation mechanism. The maximum velocity appears just to the right of the anode/separator interface, and it is close in value to the maximum in the base case model.

The convection analysis presented by Paxton and Newman [36] for the nickel/metal hydride system is applied to the binary model. The results are similar. The migration flux is dominant and is about twice the maximum diffusion flux based on the separator porosity, with the migration flux on the order of  $10^{-6}$  mol/cm<sup>2</sup> s. The convection flux based on the maximum velocity is on the order of  $10^{-7}$  mol/cm<sup>2</sup> s. For various calculations of a total electrolytic flux based on different porosity and concentration gradient values, the convective flux is always below 10% of the total flux. This criterion was used by Paxton and Newman to justify neglecting convection in the model. A future binary electrolyte model can be simplified by ignoring the convective effects.

The assumption of direct ZnO formation in the anode with the binary model gives very different porosity profiles when compared to the ternary model. Fig. 7 shows the porosity profiles for the entire cell. The cathode profiles do

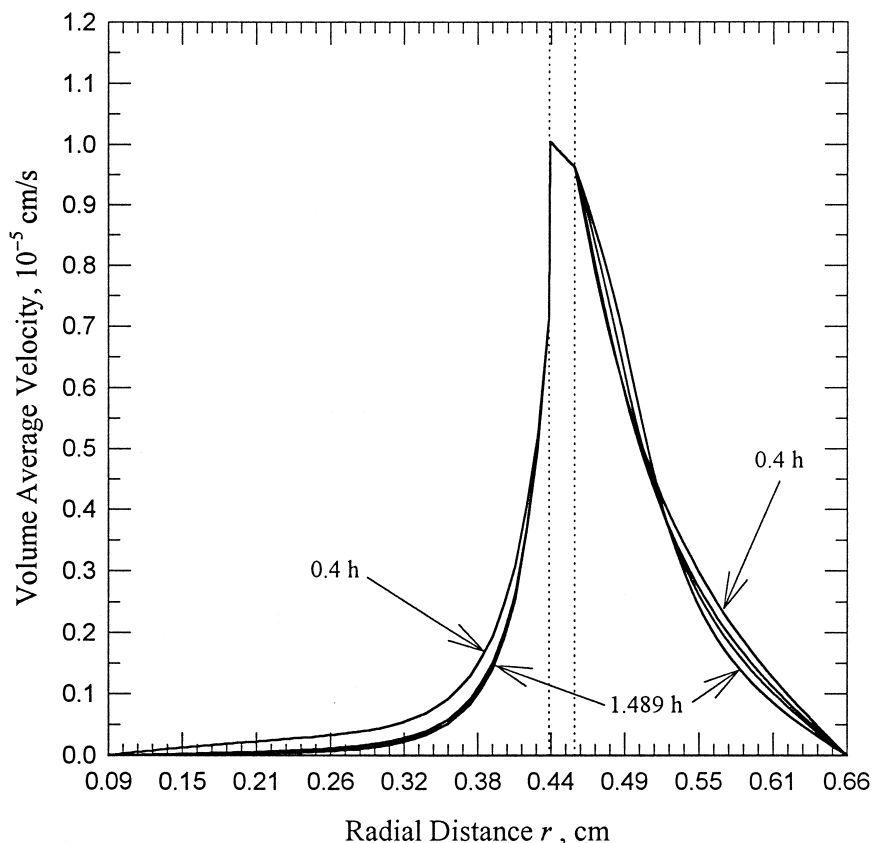


Fig. 6. Electrolyte velocity profiles calculated with the binary electrolyte model.

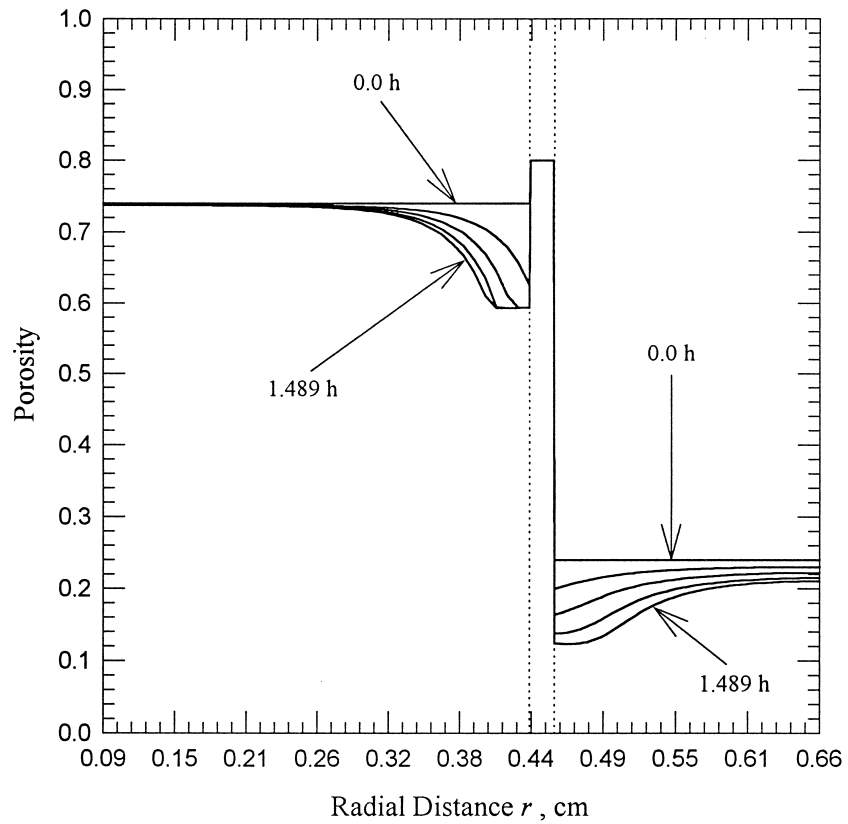


Fig. 7. Porosity profiles calculated with the binary electrolyte model.

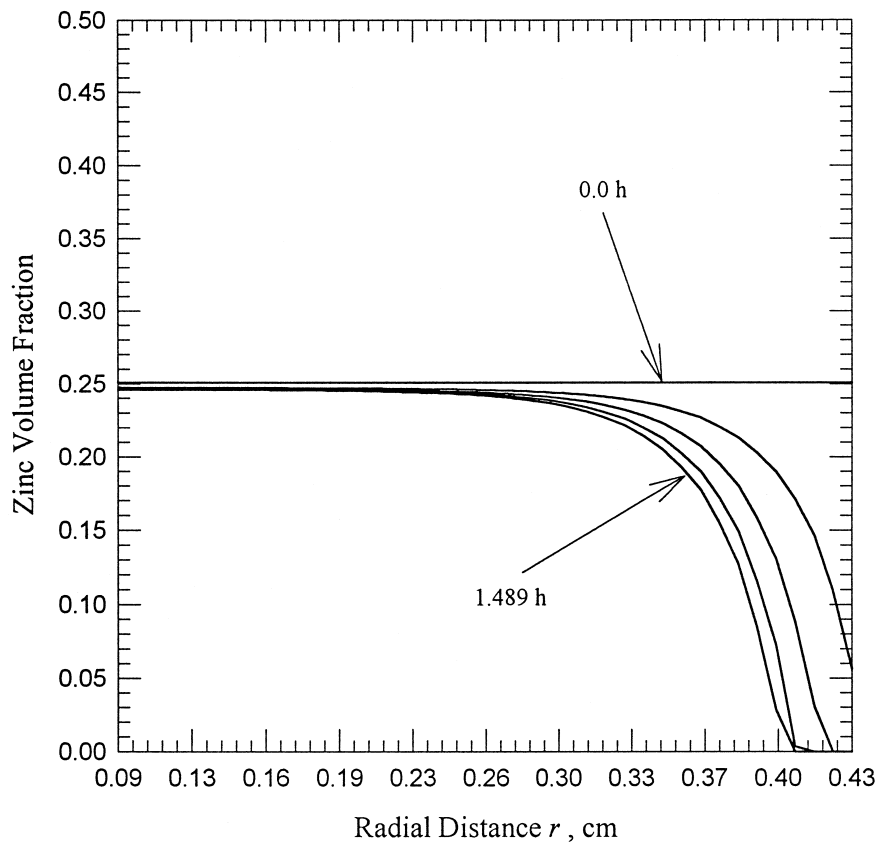


Fig. 8. Zinc volume fraction profiles in the anode, calculated with the binary electrolyte model.

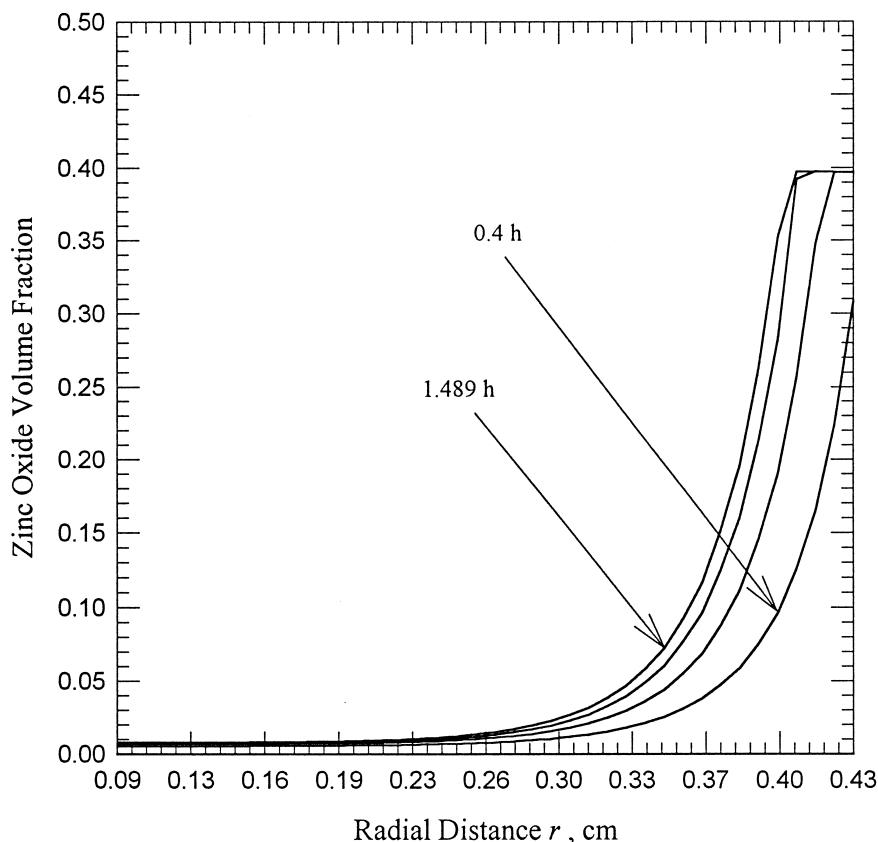


Fig. 9. Zinc oxide volume fraction profiles in the anode, calculated with the binary electrolyte model.

not change with respect to the base case model, so they are not discussed further. There is no precipitation in the separator and the porosity is constant in this region. This is contrasted with the  $\epsilon_s$  value of less than 20% to the right of the anode/separator interface in the base case model. With the original dissolution–precipitation model, the anode porosity near the anode/separator interface increases because of Zn oxidation to zincate ion. The binary electrolyte model calculates direct ZnO formation at all locations in the anode, and the porosity decreases near the anode/separator interface because the partial molar volume of ZnO is larger than the value for Zn.

Between 0.4 and 0.8 h, the porosity values near the anode/separator interface remain constant because all of the Zn at this location is reacted to form ZnO. This corresponds to 100% utilization, which is not observed with the ternary model. A minimum attainable porosity of about 59% is achieved. An advantage of the binary model is that there are well-defined limits on the porosity variation in the anode. The anode reaction dynamics are easier to follow as a result of this. The direct ZnO formation is a less dramatic formulation because the porosity variations are not as complex as with the dissolution–precipitation mechanism. There is little porosity variation in the anode interior because of the small penetration depth of the

electrochemical reaction. The Zn and ZnO volume fraction profiles in the anode are shown in Figs. 8 and 9, respectively. Figs. 8 and 9 conform to the overall porosity curves.

An important feature in Figs. 7–9 is the relation to the anodic transfer current profiles, which are nearly constant after the start of discharge. There is no reaction front that moves through the anode towards the anode current collector. The volume fraction profiles do not represent a front-like reaction trend. Instead, they reflect the consumption behavior and product formation characteristics of a position-dependent but time-independent electrochemical reaction rate in this region. The Zn utilization is minimal to the

Table 2  
Quantities used in the current distribution analysis

$\alpha_a$ anode	1.0
$\alpha_c$ anode	1.0
$i_0$ anode	0.06 A/cm <sup>2</sup> [1]
$L$	4.15 cm [1]
$T^0$	298.15 K [1]
$I$	1.0 A
$\kappa^0$	0.6 $\Omega^{-1}$ cm <sup>-1</sup> [30]
$\sigma_a^0$	$2.30 \times 10^4$ $\Omega^{-1}$ cm <sup>-1</sup>

Table 3  
Results from the binary electrolyte model application

$a_a^0$ (cm <sup>-1</sup> )	$\nu^2$	$t_d$ (h)	$f_d$
1.0	1.430	1.283	0.500
10.0	14.30	1.444	0.563
50.0	71.52	1.489	0.580
100.0	143.0	1.494	0.582
1000.0	$1.430 \times 10^3$	1.478	0.575
$1.0 \times 10^4$	$1.430 \times 10^4$	1.456	0.567

left of the radial location where  $j_a$  tapers off. This is depicted in Figs. 7–9.

## 5. Model application

The original ternary model is highly sensitive to selected values of  $a_a^0$ , the initial specific interfacial area in the anode. Raising this value above the original model value also causes simulated zincate ion depletion, and thus voltage fluctuations, in the ternary model. A range of  $a_a^0$  values from 1.0 to 1000.0 cm<sup>-1</sup> is too broad for the ternary model to handle without numerical problems. The binary model is used here to screen different  $a_a^0$  values without the possibility of zincate ion effects.

A current distribution analysis [5,16,37] is performed for the anode with respect to  $a_a^0$ . The three important parameters are a dimensionless cell current

$$\delta = \frac{\alpha_a FI(r_a - r_{ac})}{RT^0 2\pi \left(\frac{r_{ac} + r_a}{2}\right) L} \left( \frac{1}{\kappa^0 (\epsilon_a^0)^{1.5}} + \frac{1}{\sigma_a^0} \right) \quad (19)$$

a dimensionless exchange current density

$$\nu^2 = \frac{(\alpha_a + \alpha_c) Fa_a^0 i_0 (r_a - r_{ac})^2}{RT^0} \left( \frac{1}{\kappa^0 (\epsilon_a^0)^{1.5}} + \frac{1}{\sigma_a^0} \right) \quad (20)$$

and the ratio of the effective matrix conductivity to the effective electrolyte conductivity

$$\gamma = \frac{\sigma_a^0}{\kappa^0 (\epsilon_a^0)^{1.5}} \quad (21)$$

where  $I$  is the cell current, and  $\sigma_a^0$  is the initial effective matrix conductivity in the anode. When either  $\delta$  or  $\nu^2$  is much larger than unity, the reaction distribution in the anode is nonuniform. If  $\gamma$  is much greater than unity, the reaction is skewed towards the anode/seperator interface.

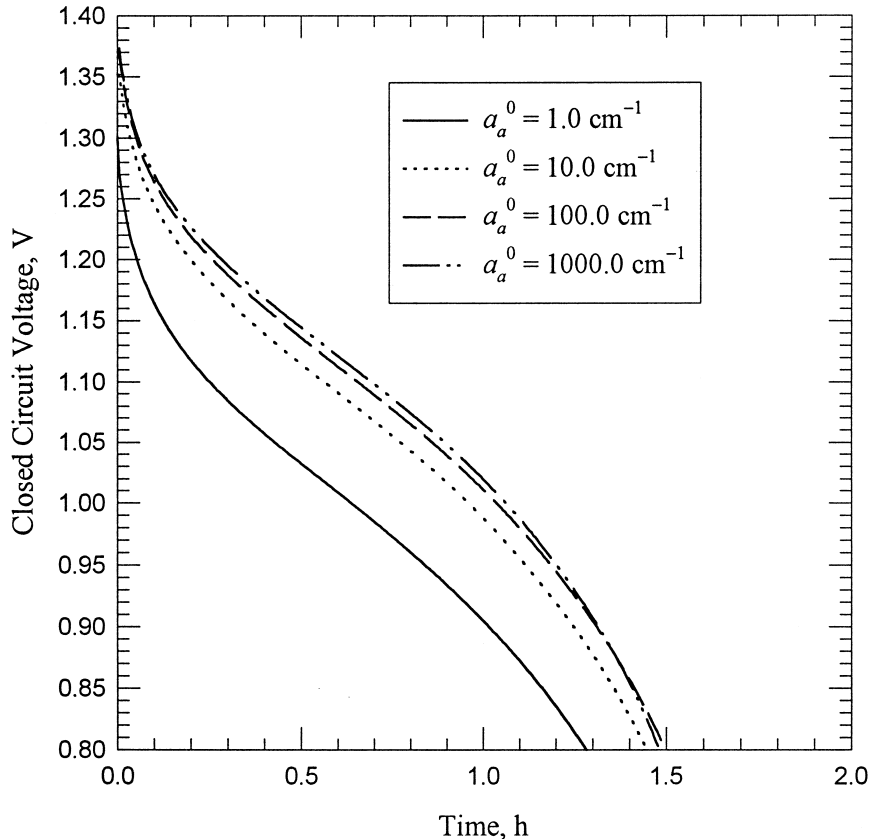


Fig. 10. Cell voltage curves from the binary electrolyte model application.

Table 2 lists the values needed in calculating the three parameters, where Table 1 gives the base case  $a_a^0$  value. Only  $\nu^2$  varies with  $a_a^0$ . The other two parameter values are fixed, with  $\delta = 5.09$  and  $\gamma = 6.03 \times 10^4$ . The  $\delta$  value is not conclusive, but  $\gamma$  is extremely large and the anode reaction rate is largest near the anode/separator interface. Simulations are performed with the binary electrolyte model for various  $a_a^0$  values, with the  $\nu^2$  values and discharge times listed in Table 3. Values of  $f_d$ , the depth of discharge at the cell cutoff voltage, are also shown.

For the base case with  $a_a^0 = 50 \text{ cm}^{-1}$ ,  $\nu^2 = 71.5$  and the transfer current is highly nonuniform and maximized near the anode/separator interface. This is supported by Fig. 3. As  $a_a^0$  is increased,  $\nu^2$  increases, and the transfer current should become more nonuniform. Fig. 10 shows the cell voltage curves for the  $a_a^0$  values in Table 3, except for the  $a_a^0 = 50 \text{ cm}^{-1}$  and  $a_a^0 = 1.0 \times 10^4 \text{ cm}^{-1}$  simulations. The operating voltage and discharge time rise largely when  $a_a^0$  is increased from 1.0 to 10.0  $\text{cm}^{-1}$ . Between 10.0 and 100.0  $\text{cm}^{-1}$ , the cell life increase is less noticeable. Above  $a_a^0 = 100.0 \text{ cm}^{-1}$ , the discharge time decreases from the maximum achieved with  $a_a^0 = 100.0 \text{ cm}^{-1}$ . The maximum depth of discharge is close to 60%.

The binary electrolyte model predicts very low anode polarization with the base case  $a_a^0$  value. Raising  $a_a^0$  above the base case value does not have a large performance effect because the relative decrease in the total anode overpotential is small, at the expense of a highly nonuniform reaction rate in the anode. Thus, the cell life begins to decrease when  $a_a^0$  is too large. The results presented here are useful because the effect of  $a_a^0$  changes in the ternary model is also expected to be small. However, the ternary model is too sensitive with respect to  $a_a^0$  to show this behavior. The binary electrolyte model is flexible enough to prove that  $a_a^0$  should not be a crucial parameter for normal ranges in value.

## 6. Conclusions

This study demonstrates the successful revision of a cell model based on a physical analysis, so that numerical discrepancies can be removed while observing more consistent discharge phenomena. The binary electrolyte model is useful for a number of reasons. Most importantly, there are no numerical problems associated with the zincate ion. Also, the physical property data for the binary system are more cohesive. The assumption of a binary system is made plausible by physical arguments based on the precipitation of ZnO, and because of the limitations of the ternary model. The anode behavior is simplified. This is more rational because of the low voltage drop in this region. The simulated results are a higher operating voltage and longer cell life for the test discharge rate. The reaction distribution and overpotential profiles in the anode maintain the same characteristics from the original model. The porosity

variation is less complex in the anode and separator, and the full utilization of Zn near the anode/separator interface is calculated. This is contrasted with the volume fraction profiles predicted by the dissolution–precipitation mechanism. A model application shows the flexibility of the binary model when it is used in the screening of parameters that cause numerical difficulties with the ternary model.

## 7. List of symbols

$a_a$	Specific interfacial area in the anode ( $\text{cm}^{-1}$ )
$a_c$	Specific interfacial area in the cathode ( $\text{cm}^{-1}$ )
$a_s$	Specific interfacial area in the separator ( $\text{cm}^{-1}$ )
$c_i$	Concentration of species $i$ ( $\text{mol}/\text{cm}^3$ )
$c_{i,\text{ref}}$	Reference concentration of species $i$ ( $\text{mol}/\text{cm}^3$ )
$D_i$	Diffusion coefficient of aqueous salt $i$ ( $\text{cm}^2/\text{s}$ )
$Da$	Damköhler number
$f_B$	Mean molar activity coefficient of the KOH electrolyte
$f_d$	Depth of discharge at the cell cutoff voltage
$F$	Faraday's constant (96,487 C/mol)
$\mathbf{I}$	Cell current density vector ( $\text{A}/\text{cm}^2$ )
$I$	Cell current (A)
$i_0$	Anode exchange current density at a reference condition ( $\text{A}/\text{cm}^2$ )
$i_2$	Superficial current density in the solution phase ( $\text{A}/\text{cm}^2$ )
$j_a$	Transfer current in the anode ( $\text{A}/\text{cm}^3$ )
$j_c$	Transfer current in the cathode ( $\text{A}/\text{cm}^3$ )
$k_s$	Dissolution or precipitation rate constant for the ZnO precipitation reaction in the anode ( $\text{cm}/\text{s}$ )
$k_x$	Chemical rate constant for the dissolution or precipitation of ZnO ( $\text{cm}/\text{s}$ )
$L$	Cell height (cm)
$n$	Number of electrons transferred in the reference electrode reaction
$N_2$	Molar flux of hydroxyl ion ( $\text{mol}/\text{cm}^2 \text{ s}$ )
$r_i$	Current collector location $i$ , or electrode/separator interface location $i$ (cm)
$R$	Universal gas constant (8.3143 J/mol K)
$R_{p,a}$	Intrinsic precipitation rate in the anode ( $\text{mol}/\text{cm}^3 \text{ s}$ )
$R_{p,s}$	Intrinsic precipitation rate in the separator ( $\text{mol}/\text{cm}^3 \text{ s}$ )
$s_i$	Stoichiometric coefficient of species $i$ in the reference electrode reaction
$t$	Time (s)
$t_d$	Discharge time to reach the cutoff voltage (h)
$t_{\text{diff},a}$	Time scale for zincate ion diffusion in the anode (s)
$t_{\text{diff},s}$	Time scale for zincate ion diffusion in the separator (s)
$t_{p,a}$	Time scale for precipitation in the anode (s)
$t_{p,s}$	Time scale for precipitation in the separator (s)

$t_2$	Hydroxyl ion transference number with respect to the volume average velocity
$T$	Cell temperature (K)
$\bar{v}$	Volume average velocity in the electrolyte (cm/s)
$\bar{V}_i$	Partial molar volume of species $i$ (cm <sup>3</sup> /mol)
$z_2$	Hydroxyl ion charge number

*Greek*

$\alpha_a$	Anodic transfer coefficient for the anode electrochemical reaction
$\alpha_c$	Cathodic transfer coefficient for the anode electrochemical reaction
$\gamma$	Ratio of matrix to electrolyte effective electrical conductivities in the anode
$\delta$	Dimensionless cell current using anode parameters
$\epsilon$	Porosity
$\epsilon_i$	Porosity of region $i$ , or solid volume fraction of species $i$
$\eta$	Local overpotential (V)
$\kappa$	Electrolyte conductivity ( $\Omega^{-1} \text{ cm}^{-1}$ )
$\nu$	Square root of the dimensionless exchange current density in the anode
$\nu_e$	Number of ions that can dissociate from the binary aqueous salt
$\nu_{ij}$	Number of ions of species $i$ contained in one molecule of salt $j$
$\sigma$	Effective matrix conductivity ( $\Omega^{-1} \text{ cm}^{-1}$ )
$\sigma_a$	Anode effective matrix conductivity ( $\Omega^{-1} \text{ cm}^{-1}$ )

*Main subscripts*

A	Potassium zincate
B	Potassium hydroxide
0	Solvent (water)
1	Zincate ion
2	Hydroxyl ion

*Superscripts*

0	Initial condition or characteristic value
---	---

**References**

- [1] E.J. Podlaha, H.Y. Cheh, J. Electrochem. Soc. 141 (1994) 15.
- [2] E.J. Podlaha, H.Y. Cheh, J. Electrochem. Soc. 141 (1994) 28.
- [3] J.J. Kriegsmann, H.Y. Cheh, J. Power Sources 84 (1999) 114.
- [4] J.J. Kriegsmann, H.Y. Cheh, J. Power Sources 84 (1999) 52.
- [5] J.-S. Chen, H.Y. Cheh, J. Electrochem. Soc. 140 (1993) 1205.
- [6] J.-S. Chen, H.Y. Cheh, J. Electrochem. Soc. 140 (1993) 1213.
- [7] W. Tiedemann, J. Newman, J. Electrochem. Soc. 122 (1975) 1482.
- [8] J. Newman, J. Electrochem. Soc. 142 (1995) 97.
- [9] M. Doyle, J. Newman, J. Power Sources 54 (1995) 46.
- [10] M. Doyle, J. Newman, J. Appl. Electrochem. 27 (1997) 846.
- [11] R. Darling, J. Newman, J. Electrochem. Soc. 144 (1997) 3057.
- [12] R. Darling, J. Newman, J. Electrochem. Soc. 144 (1997) 4201.
- [13] R. Darling, J. Newman, J. Electrochem. Soc. 145 (1998) 990.
- [14] R. Pollard, J. Newman, J. Electrochem. Soc. 128 (1981) 491.
- [15] M. Doyle, T.F. Fuller, J. Newman, J. Electrochem. Soc. 140 (1993) 1526.
- [16] T.F. Fuller, M. Doyle, J. Newman, J. Electrochem. Soc. 141 (1994) 1.
- [17] K.W. Choi, D.N. Bennion, J. Newman, J. Electrochem. Soc. 123 (1976) 1616.
- [18] K.W. Choi, D. Hamby, D.N. Bennion, J. Newman, J. Electrochem. Soc. 123 (1976) 1628.
- [19] W.G. Sunu, D.N. Bennion, J. Electrochem. Soc. 127 (1980) 2007.
- [20] W.G. Sunu, D.N. Bennion, J. Electrochem. Soc. 127 (1980) 2017.
- [21] R.E.F. Einerhand, W. Visscher, J.J.M. de Goeij, E. Barendrecht, J. Electrochem. Soc. 138 (1991) 1.
- [22] R.E.F. Einerhand, W. Visscher, J.J.M. de Goeij, E. Barendrecht, J. Electrochem. Soc. 138 (1991) 7.
- [23] W.G. Sunu, PhD Thesis, University of California, Los Angeles, CA, 1978.
- [24] J.S. Newman, Electrochemical Systems, 2nd edn., Prentice-Hall, Englewood Cliffs, NJ, 1991.
- [25] O. Söhnel, J. Garside, Precipitation — Basic Principles and Industrial Applications, Butterworth–Heinemann, Boston, MA, 1992.
- [26] A.E. Nielsen, Kinetics of Precipitation, Macmillan, New York, 1964.
- [27] J.M. Heikonen, H.J. Ploehn, R.E. White, J. Electrochem. Soc. 145 (1998) 1840.
- [28] D.F. Boucher, G.E. Alves, Chem. Eng. Prog. 55 (1959) 55.
- [29] J.J. Kriegsmann, H.Y. Cheh, J. Power Sources 77 (1999) 127.
- [30] J.J. Kriegsmann, H.Y. Cheh, J. Power Sources 79 (1999) 262.
- [31] T.I. Evans, T.V. Nguyen, R.E. White, J. Electrochem. Soc. 136 (1989) 328.
- [32] D. Fan, PhD Thesis, Texas A&M University, College Station, TX, 1991.
- [33] E.J. Podlaha, PhD Thesis, Columbia University, New York, 1992.
- [34] J. Van Zee, G. Kleine, R.E. White, J. Newman, in: R.E. White (Ed.), Electrochemical Cell Design, Plenum, New York, pp. 377–389, 1984.
- [35] D.N. Bennion, AIChE Symp. Ser. 79 (1983) 25.
- [36] B. Paxton, J. Newman, J. Electrochem. Soc. 144 (1997) 3818.
- [37] J. Newman, W. Tiedemann, AIChE J. 21 (1975) 25.